Langmuir

Article

pubs.acs.org/Langmuir

Numerical Study of the Most Stable Contact Angle of Drops on Tilted Surfaces

J. A. White,*[,†,§] M. J. Santos,[†] M. A. Rodríguez-Valverde,[‡] and S. Velasco[†,§]

[†]Department of Applied Physics, University of Salamanca, 37008 Salamanca, Spain

[‡]Biocolloid and Fluid Physics Group, Department of Applied Physics, University of Granada, Campus de Fuentenueva, E-18071 Granada, Spain

ABSTRACT: We present results for the most stable contact angle using a numerical implementation of the tilting plate method of Montes et al. (Montes Ruiz-Cabello, F. J.; Rodriguez-Valverde, M. A.; Cabrerizo-Vilchez, M. *Soft Matter* **2011**, *7*, 10457−10461). Comparison with the experimental results is made, obtaining a good agreement in most situations. In addition, the evolution of the contact angles of a tilted drop with a fixed circular line is analyzed. This analysis allows one to theoretically predict the most stable contact angle for tilted drops.

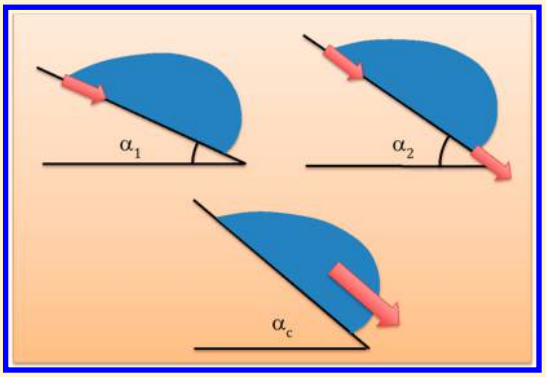

1. INTRODUCTION

Young's equation[1] determines a unique value for the equilibrium contact angle of a liquid−vapor interface with an *ideal* solid surface. This value is the Young contact angle θ_Y and characterizes the equilibrium state of the solid−liquid−vapor system since it gives rise to the minimum of the Gibbs energy.[2] Consequently, a unique contact angle θ_Y is expected for ideal systems. This contradicts the experimental observation for most *real* systems where a range of contact angles is obtained.[3−5] This implies that the triple phase contact line for a real system is pinned for contact angles in the range

$$\theta_{rec} < \theta < \theta_{adv} \quad (1)$$

where θ_{adv} and θ_{rec} are the advancing and receding contact angles that can be measured in an advancing and a receding triple line, respectively.[3−5] The multiplicity of contact angles given by eq 1 is called contact angle hysteresis and has been the subject of extensive study in the past several decades (see the recent review of Eral et al.[6] and references therein). A theoretical explanation of contact angle hysteresis can be obtained by assuming that the Gibbs energy of the system has multiple minima and a single global minimum. Within this theoretical picture, each allowed contact angle corresponds to a metastable state of the system and the global equilibrium is given by the so-called most stable contact angle.[2]

One way to access experimentally the most stable contact angle is to apply vertical vibrations to drops and menisci[7−12] in such a way that the energy barriers in the metastable states are overcome and the system can eventually reach the global equilibrium. Montes et al.[13] suggest a different approach by considering that the most stable state can be identified as the configuration with the lowest susceptibility to a given mechanical perturbation. This mechanical perturbation can be a vertical vibration, but there are other possibilities like the tilted plate method for evaluating the most stable contact angle.[14] As we shall see below in more detail, in this method, one looks for the drop with the initial contact angle that allows to obtain the maximum tilt angle without displacement of the contact line. From the approach of Montes et al.[13] one might infer that there is a *different* most stable contact angle associated with each *different* mechanical perturbation (vibration, tilting, etc.). Unless otherwise specified, in what follows, we shall refer to the most stable contact angle as the one obtained in a tilting situation.

The goal of this paper is to perform a numerical analysis of the tilted plate method based on Surface Evolver calculations.[15] To perform such calculations in the Surface Evolver framework, we have considered an algorithm[16] that allows for an appropriate description of contact angle hysteresis and, consequently, of the retention forces arising in nonaxisymmetric liquid drops resting on inclined surfaces.[17] In this context, it is worth mentioning that other algorithms have been recently developed for describing tilted drops with Surface Evolver.[18−20]

This work is structured as follows. In section 2, we briefly describe the main features of the experimental tilting plate method and then we show how the method can be numerically implemented in Surface Evolver with a good agreement with the experimental results obtained for the most stable contact angle. Motivated by the results of section 2, in section 3, we

Received: July 25, 2014
Revised: April 15, 2015

DOI: 10.1021/acs.langmuir.5b00834
Langmuir XXXX, XXX, XXX−XXX

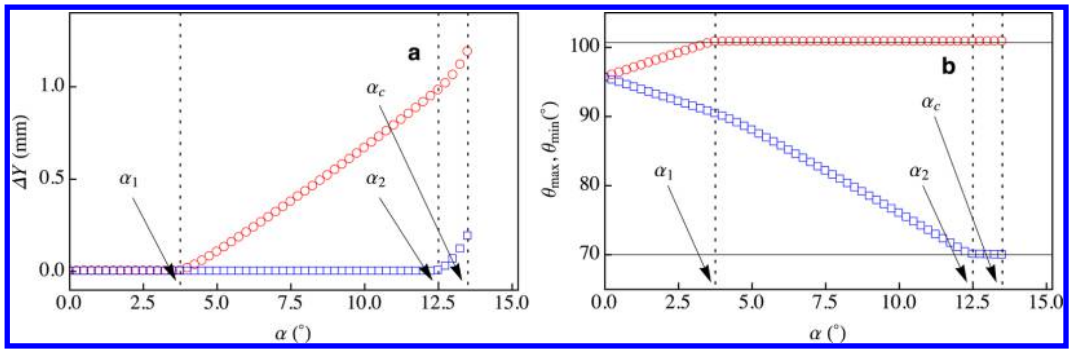

Figure 1. Numerical results for a 150 μL water drop on the PP surface with an initial contact angle $\theta_0 = 96°$. (a) Displacement ΔY of the downhill (circles) and uphill (squares) contact line points versus the tilt angle α. (b) Maximum (circles) and minimum (squares) contact angles versus α. The dotted vertical lines indicate the positions of the critical tilt angles α_1, α_2, and α_c. The solid lines in (b) show the receding and advancing contact angles for this system, $\theta_{rec} = 70°$ and $\theta_{adv} = 100.7°$.

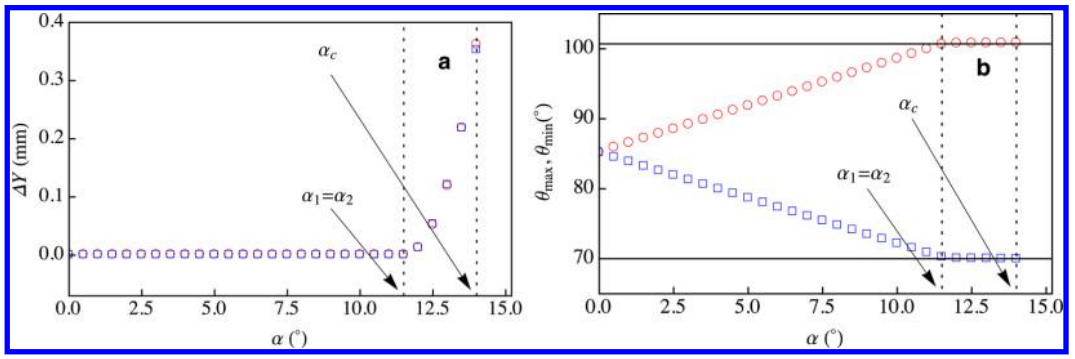

Figure 2. Same as Figure 1, but for an initial contact angle $\theta_0 = 85.1°$, equal to the most stable contact angle of the system. Note the change in vertical scale in (a).

study the evolution of the contact angles in a tilted drop with a pinned contact line. From this study, we develop theoretical expressions for the most stable contact angle in the tilting plate method. We conclude with a brief summary of our main results.

2. EVALUATION OF THE MOST STABLE CONTACT ANGLE FROM A NUMERICAL IMPLEMENTATION OF THE TILTED PLATE METHOD

Let us consider an axisymmetric sessile drop placed on an horizontal smooth flat surface with an initial contact angle θ_0. Assuming that $\theta_{rec} < \theta_0 < \theta_{adv}$, if the substrate is slowly tilted, for sufficiently small tilt angles, the triple contact line has a circular shape and is pinned to the surface. Depending on the initial conditions of the system, for larger tilt angles, one can observe the displacement of either the rear (uphill) or the front (downhill) part of the contact line. At even larger tilt angles, the drop begins to slide. According to this behavior, the following critical tilt angles have been identified:[14]

- α_1: Critical tilt angle for which the first displacement of the contact line is observed regardless of whether the displacement occurs at the rear or at the front of the drop.
- α_2: Critical tilt angle for which both the uphill and the downhill parts of the contact line are displaced.
- α_c: Critical tilt angle for drop sliding.

As shown experimentally[14] and numerically,[17] the values of these critical angles are strongly dependent on the initial contact angle θ_0 at zero tilt. The experimental method recently proposed by Montes et al.[14] considers drops with different values of the initial contact angle belonging to the range $\theta_{rec} < \theta_0 < \theta_{adv}$. We note that these values of θ_0 are achieved experimentally by adding and subtracting liquid to the drop which is initially placed on an horizontal plate. For each value of θ_0, the plate is slowly tilted at constant rate until measuring α_1 and α_2. Montes et al.[14] suggest that the initial contact angle that leads to a maximum value for α_1 provides a good estimate of the most stable contact angle of the system. Furthermore, in this situation, the measured values of α_1 and α_2 are very close so that $\alpha_2 - \alpha_1$ reaches its minimum value, near zero.

In what follows, we show how this experimental method can also be numerically implemented by means of the finite-elements software Surface Evolver[15] in which local constraints are included for incorporating the contact angle hysteresis required to correctly describe a drop on an inclined surface.[16,17] The Surface Evolver program represents the drop interface by means of a triangular tessellation in terms of vertices, edges, and facets. In our simulations, we have considered a mesh with 505 vertices, 1464 edges, and 960 facets which corresponds to 48 vertices located in the triple contact line. Each simulation has been made by starting from an axisymmetric drop with a given initial contact angle θ_0 that is placed on a horizontal surface which is subsequently tilted in steps of $\Delta\alpha = 0.5°$. For each tilt angle α, we perform 1000 iteration steps in order to ensure numerical convergence. Except near the critical tilt angle α_c, the convergence of the numerical procedure is granted since the relative deviation in the interfacial energy between two consecutive iteration steps is less than 10^{-7}.

To compare with the experimental results of Montes et al.,[14] in our numerical analysis, we have considered pure water drops with a volume $V = 150$ μL resting on seven different polymer surfaces: PP, PC, PET, uPVC, PTFE-s, PTFE-r, and PDMS-s.

DOI: 10.1021/acs.langmuir.5b00834
Langmuir XXXX, XXX, XXX−XXX

The relatively large drop volume considered in the experimental work of Montes et al. is due to the well established fact that drop volumes must be large enough in order to allow for realiable measurements of the receding contact angles.[21]

Figures 1 and 2 show our numerical results for the PP surface for two different values of the initial contact angle in the range $\theta_{rec} \leq \theta_0 \leq \theta_{adv}$, where $\theta_{rec} = 70°$ and $\theta_{adv} = 100.7°$ for this system.[14] In particular, we consider $\theta_0 = 96°$ in Figure 1 and $\theta_0 = 85.1°$ in Figure 2. The displacement ΔY of the uphill (downhill) contact line point for each tilt angle α is shown in Figures 1a and 2a. The behavior with the tilt angle of the minimum (maximum) value of the contact angle θ_{min} (θ_{max}) attained at the uphill (downhill) point of the contact line is shown in Figures 1b and 2b. All the calculations are made following the procedure presented in ref 17.

It should be emphasized that θ_{min} and θ_{max} must not be confused with θ_{rec} and θ_{adv}, respectively. For a given tilt angle α, θ_{min} and θ_{max} are the contact angles measured at the uphill and the downhill points of the contact line, respectively, and they happen to be the minimum and maximum contact angles of the drop for this situation. With increasing values of the tilt angle α, θ_{min} (θ_{max}) will decrease (increase) and eventually reach its minimum (maximum) value which is the receding (advancing) contact angle θ_{rec} (θ_{adv}) *for a tilted plate situation*. Of course, in most situations (see Figure 1), the advancing and receding angles are not reached for the same tilt angle. In this context, it must be mentioned that Krasovitski and Marmur[22] showed that the maximum and minimum contact angles for drops on an inclined plate do not always coincide with θ_{adv} and θ_{rec} in two-dimensional drops. This indicates that the receding or the advancing contact angles measured in a tilt experiment when incipient motion of the uphill or the downhill part of the contact line is observed might differ from the ones measured in a standard dynamic one-cycle contact angle measurement.[5] This fact does not affect the main results of this work, provided that one considers the *receding* and *advancing* angles measured in a tilted plate experiment.

Figure 1 shows a situation where the initial contact angle $\theta_0 = 96°$ is close to the advancing contact angle. For $\alpha \lesssim 3.75°$ the contact line remains pinned with a circular shape while the maximum (minimum) contact angle at the downhill (uphill) contact line point grows (decreases) in an approximately linear way (Figure 1b). At $\alpha_1 \cong 3.75°$, the maximum contact angle θ_{max} reaches the value $\theta_{adv} = 100.7°$ and one observes the incipient displacement of the downhill contact line point (Figure 1a). For $3.75° \lesssim \alpha \lesssim 12.5°$, the front of the drop is displaced while the rear remains pinned (Figure 1a); meanwhile, in Figure 1a, one can see that $\theta_{max} = \theta_{adv}$ and θ_{min} decreases with an approximate linear behavior with a slope different from that of $\alpha \lesssim 3.75°$. At $\alpha_2 \cong 12.5°$, $\theta_{min} = \theta_{av} = 70°$ and the uphill contact line point begins its displacement. We note that, for this tilt angle, although both the rear and the front of the drop are displaced, the drop does not experience global motion which occurs at $\alpha_c \cong 13.5°$.

In Figure 2, the initial contact angle $\theta_0 = 85.1°$ is chosen to be equal to the most stable contact angle of the system θ^C_{tilt} determined from the method of section 3. Consequently, for a large range of tilt angles ($\alpha \lesssim 11.6°$), the contact line remains pinned and the displacement ΔY of the uphill and downhill contact line points is equal to zero (Figure 2a) while the maximum and minimum contact angles show an approximate linear behavior (Figure 2b). At $\alpha_1 = \alpha_2 \cong 11.6°$, θ_{min} and θ_{max} simultaneously attain $\theta_{rec} = 70°$ and $\theta_{adv} = 100.7°$, respectively. At this point, both the uphill and downhill contact line points experience incipient displacement ($\Delta Y > 0$) without global motion of the drop. Again, the drop slides at a larger critical tilt angle $\alpha_c \cong 14°$.

Figure 3 shows the critical tilt angles α_1 and α_2 as a function of the initial contact angle θ_0 for a 150 μL drop of water on PP.

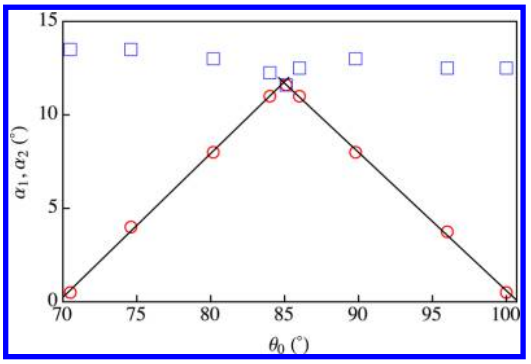

Figure 3. Critical tilt angles α_1 (circles) and α_2 (squares) versus the initial contact angle θ_0. The symbols are our numerical results for a 150 μL drop of water on PP. The solid lines are linear fits to the data.

From this figure, one observes that α_1 reaches its maximum value at an initial contact angle of $\theta_0 \approx 85°$. As expected from their definition, for each θ_0, one has that $\alpha_2 \geq \alpha_1$ but these values become equal when α_1 reaches its maximum value. The same behavior has been observed for the other polymer surfaces and agrees with experimental results.[14] According to the prescription of Montes et al.,[14] the most stable contact angle in a tilting plate experiment can be determined from the value of θ_0 that yields the maximum value of α_1; we shall denote this value as θ^A_{tilt}. Given the approximate linear behaviors obtained for α_1 in the zones below and above its maximum, an estimation of θ^A_{tilt} can be made by finding the point of intersection for the two linear fits shown in Figure 3. For this particular case of a 150 μL drop of water on PP, the maximum is located at $\theta^A_{tilt} = 84.9°$. We note that this estimation is slightly different from the value $\theta_0 = 85.1°$ considered in Figure 2. The results for θ^A_{tilt} obtained for the seven polymer surfaces considered are listed in Table 1 where we also list the experimental results of Montes et al.[14] for the advancing, receding, and most stable contact angle. For the sake of comparison, the arithmetic mean

$$\langle\theta\rangle = \frac{\theta_{adv} + \theta_{rec}}{2} \tag{2}$$

and the cosine average

$$\langle\theta_{cos}\rangle = \arccos\left(\frac{\cos\theta_{adv} + \cos\theta_{rec}}{2}\right) \tag{3}$$

are also listed in Table 1. Overall, we observe a very good agreement between experimental results and the numerical estimation of the most stable contact angle given by θ^A_{tilt}. The only remarkable discrepancy is the one obtained for the water−uPVC system. In this case, we also obtain important differences in the numerical estimation of the critical tilt angle α_1 (see the comments of Figure 4 below). As expected, the values of $\langle\theta\rangle$ and $\langle\theta_{cos}\rangle$ listed in Table 1 are also very close to θ^A_{tilt} for all cases, with important differences with θ^{exp}_{tilt} for the water-uPVC system.

DOI: 10.1021/acs.langmuir.5b00834
Langmuir XXXX, XXX, XXX−XXX

Table 1. Advancing θ_{adv} and Receding θ_{rec} Contact Angles,[14] Their Arithmetic Mean $\langle\theta\rangle$, Their Cosine Average $\langle\theta_{cos}\rangle$, the Experimentally Most Stable Contact Angle for the Tilting Plate Method[14] θ^{exp}_{tilt}, and the Results of the Numerical Calculations θ^{A}_{tilt}, θ^{C}_{tilt}, and $\theta^{C,1}_{tilt}$ for 150 μL Water Drops on Some of the Polymer Surfaces Considered in Ref 14[a]

polymer	θ_{adv} (deg)	θ_{rec} (deg)	$\langle\theta\rangle$ (deg)	$\langle\theta_{cos}\rangle$ (deg)	θ^{exp}_{tilt} (deg)	θ^{A}_{tilt} (deg)	θ^{C}_{tilt} (deg)	$\theta^{C,1}_{tilt}$ (deg)
PP	100.7 ± 1.6	70 ± 3	85.4	85.5	86.3 ± 1.9	84.9	85.1	85.2
PC	86.2 ± 1.5	48 ± 2	67.1	68.4	65.2 ± 1.8	67.1	66.9	67.0
PET	80 ± 2	49.7 ± 1.5	64.9	65.8	65.5 ± 1.2	64.9	64.7	64.8
uPVC	86 ± 2	50 ± 2	68.0	69.1	60.2 ± 1.0	68.0	67.8	67.9
PTFE-s	110 ± 4	95.6 ± 1.0	102.8	102.7	103 ± 3	102.7	102.7	102.7
PTFE-r	126 ± 2	87.9 ± 1.3	107.0	106.0	106 ± 2	106.3	106.3	106.3
PDMS-s	120.2 ± 1.9	65.2 ± 1.9	92.7	92.4	93 ± 3	91.3	91.8	91.9

[a] θ^{A}_{tilt} is the result of the approach presented in Figure 3, θ^{C}_{tilt} is the result of the solution of eqs 22−25, and $\theta^{C,1}_{tilt}$ is the first order result given by eq 26 (see text).

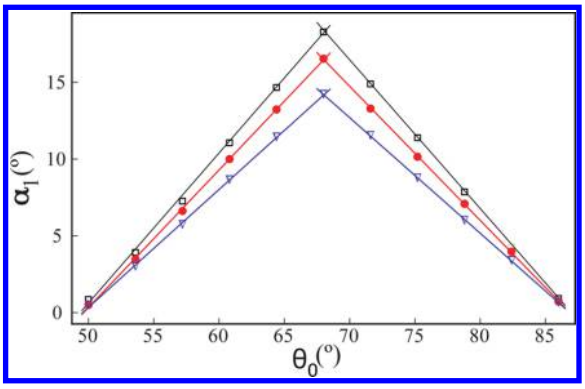

Figure 4. Critical tilt angle α_1 versus the initial contact angle θ_0. The symbols are numerical results for water drops on uPVC with volumes V = 100 μL (squares), V = 120 μL (circles), and V = 150 μL (triangles). The solid lines are linear fits to the data.

Figure 4 shows the behavior of the critical tilt angle α_1 with the initial contact angle θ_0 for 100, 120, and 150 μL water drops on uPVC. One can observe that in all cases the maximum value of α_1 is attained at $\theta^{A}_{tilt} \cong 68.0°$. Of course, the maximum values of α_1 depend on the drop volume, with a larger value for the smaller drop. It is remarkable that, for the volumes considered, we obtain results with very scarce volume dependence, in accordance with experimental measurements.[14]

Comparing Figure 4 with Figure 6a of ref 14 we observe that the experimental critical tilt angles α_1 for the water−uPVC system are much larger than those obtained numerically in the present work. We do not have a conclusive explanation for this behavior, but it could be due to an anomalous solid−liquid interaction for this system. We also note that in our calculations we used the values θ_{adv} = 86°, θ_{rec} = 50° measured by low rate dynamic contact angle experiments,[14] whereas in Figure 6 of ref 14 one can see the measurement of contact angles below 50°. Much smaller discrepancies are observed in Figure 3 that shows slightly larger values for α_1 than those plotted in Figure 3 of ref 14.

3. CONTACT ANGLE EVOLUTION IN A PINNED TILTED DROP

In the preceding section, we have seen how the most stable contact angle is determined from $\alpha_1 = \alpha_2$ so that the maximum and minimum contact angles attain the advancing and receding values, respectively, at the same tilt angle. This means that for lower inclinations the triple contact line remains pinned, with a circular shape. Consequently, one can perform an analysis of the most stable contact angle by studying the evolution of the contact angles in a tilted drop with a fixed, circular triple contact line. For this system, the following equation relating the tilt angle α and the maximum (θ_{max}) and minimum (θ_{max}) contact angles was recently derived:[17]

$$\frac{\rho g V \sin\alpha}{\sigma_{lv}\omega} = \frac{\pi}{2}(\cos\theta_{min} - \cos\theta_{max}) \equiv \frac{\pi}{2}\Delta\cos\theta \tag{4}$$

where ρ is the density of the liquid, g is the acceleration of gravity, V is the volume of the drop, σ_{lv} is the liquid−vapor surface tension, and ω is the radius of the circular contact line. In addition to this equation, approximate linear relations between sin α and either cos θ_{min} or cos θ_{max} were obtained from an analysis of Surface Evolver results[17] so that one can write in a convenient form

$$\frac{\rho g V \sin\alpha}{\sigma_{lv}\omega} \cong \frac{\pi}{2k_1}(\cos\theta_{min} - \cos\theta_0) \tag{5}$$

$$\frac{\rho g V \sin\alpha}{\sigma_{lv}\omega} \cong -\frac{\pi}{2k_2}(\cos\theta_{max} - \cos\theta_0) \tag{6}$$

where k_1 and k_2 are positive constants, and, comparing with eq 4, one obtains

$$k_1 + k_2 = 1 \tag{7}$$

Furthermore, from eqs 4−6, one has

$$\cos\theta_{min} \cong \cos\theta_0 + k_1\Delta\cos\theta \tag{8}$$

$$\cos\theta_{max} \cong \cos\theta_0 - k_2\Delta\cos\theta \tag{9}$$

which state that the cosines of the minimum and maximum contact angles in a pinned drop are approximately proportional to the cosine difference $\Delta\cos\theta$. In order to test these approximate results, we have considered a Surface Evolver simulation for a 150 μL water drop initially placed on an horizontal surface with contact angle θ_0 = 60° and circular contact line. The drop is subsequently tilted by keeping fixed the contact line; that is, the drop is *pinned* to the tilted surface. For each tilt angle, the cosines of the maximum and minimum contact angles are measured and plotted in Figure 5 against the cosine difference. As shown in Figure 5, a linear fit to the Surface Evolver results (dashed lines) provides a fairly good approximation for the behavior of cos θ_{min} and cos θ_{max}; however small deviations from the linear behavior are observed. Furthermore, for the case considered in Figure 5 with θ_0 = 60°, we obtain k_1 = 0.41726 and k_2 = 0.58274 with an estimated value for cos θ_0 equal to 0.513899, with a relative deviation of 2.8% with respect to the exact value (cos θ_0 = 0.5). The observed deviations become more apparent if we consider that

DOI: 10.1021/acs.langmuir.5b00834
Langmuir XXXX, XXX, XXX−XXX

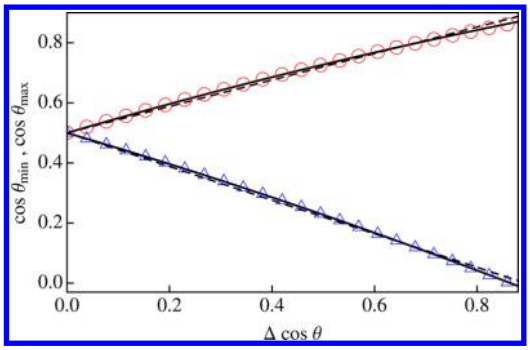

Figure 5. $\cos\theta_{min}$ (circles) and $\cos\theta_{max}$ (squares) versus the cosine diference $\Delta\cos\theta = \cos\theta_{min} - \cos\theta_{max}$ for a 150 μL water drop pinned to a tilted surface with initial contact angle $\theta_0 = 60°$. The symbols are Surface Evolver results. The solid lines are quadratic fits, and the dashed lines are linear fits to the data (see text).

eqs 8 and 9 would imply that the average $\langle\cos\theta\rangle \equiv (\cos\theta_{min} + \cos\theta_{max})/2$ should also behave linearly with $\Delta\cos\theta$, that is,

$$\langle\cos\theta\rangle \cong \cos\theta_0 + \frac{k_1 - k_2}{2}\Delta\cos\theta \tag{10}$$

However, as shown in Figure 6, $\langle\cos\theta\rangle$ presents a quadratic behavior with $\Delta\cos\theta$. In particular, in Figure 6b ($\cos\theta_0 = 0.5$), we obtain

$$\langle\cos\theta\rangle \cong 0.500295 + 0.00398378\Delta\cos\theta - 0.0962931(\Delta\cos\theta)^2 \tag{11}$$

$$\cong 0.500295 - 0.0962931(\Delta\cos\theta)^2 \tag{12}$$

This implies that

$$\langle\cos\theta\rangle \cong \cos\theta_0 + k(\Delta\cos\theta)^2 \tag{13}$$

where k depends on the initial contact angle θ_0 as shown in Figure 6a. Figure 6b shows that eq 13 provides a good approximation to the behavior of $\langle\cos\theta\rangle$. From eq 13 and the definition $\Delta\cos\theta \equiv \cos\theta_{min} - \cos\theta_{max}$, it is direct to obtain

$$\cos\theta_{min} \cong \cos\theta_0 + \frac{1}{2}\Delta\cos\theta + k(\Delta\cos\theta)^2 \tag{14}$$

$$\cos\theta_{max} \cong \cos\theta_0 - \frac{1}{2}\Delta\cos\theta + k(\Delta\cos\theta)^2 \tag{15}$$

where we note that taking $k = 0$ yields the first order eqs 8 and 9 with $k_1 = k_2 = 0.5$. In order to test eqs 14 and 15, the following quadratic fits to the Surface Evolver data (solid lines) have been plotted in Figure 5:

$$\cos\theta_{min} \cong 0.500295 + 0.503984\Delta\cos\theta - 0.0962931(\Delta\cos\theta)^2 \tag{16}$$

$$\cos\theta_{max} \cong 0.500295 - 0.496016\Delta\cos\theta - 0.0962931(\Delta\cos\theta)^2 \tag{17}$$

that give an improved approximation over the above-mentioned linear fits (dashed lines). We note that the quadratic fits yield $k = -0.0962931$, with the linear terms very close to the expected value (0.5) and an excellent estimation of $\langle\cos\theta\rangle(0.500295)$, with a relative deviation of 0.06%.

3.1. Analisys of the Parameter *k*. Figure 7 presents Surface Evolver results for the parameter k in eqs 13−15 for water drops with different volumes V = 5, 10, 17, 30, 56, and 150 μL, and different values of the initial contact angle θ_0= 60°, 70°, 80°, 90°, 100°, 110°, and 120° (from bottom to top). For each value of θ_0, we obtain that k scales with the volume according to the following power law:

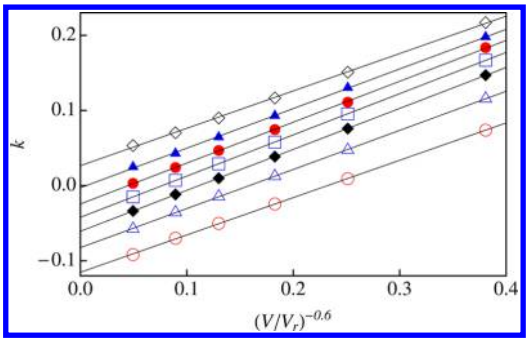

Figure 7. Parameter k versus $(V/V_r)^{-0.6}$ for water drops pinned to a tilted surface with different initial contact angles θ_0 (see text). From bottom to top θ_0 = 60°, 70°, 80°, 90°, 100°, 110°, and 120°. The symbols are Surface Evolver results. The solid lines are linear fits to the data. V_r = 1 μL.

$$k(\theta_0, V) - k_\infty(\theta_0) \cong b(\theta_0)\left(\frac{V}{V_r}\right)^{-0.6} \tag{18}$$

where

$$k_\infty(\theta_0) = \lim_{V\to\infty} k(\theta_0, V) \tag{19}$$

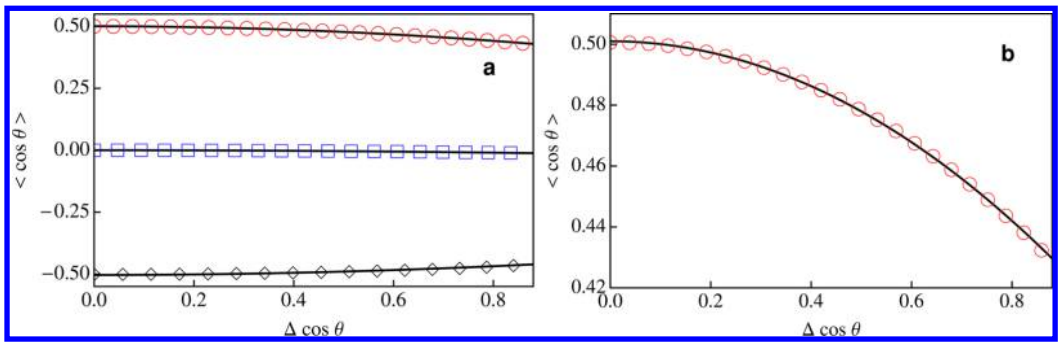

Figure 6. Behavior of $\langle\cos\theta\rangle \equiv (\cos\theta_{min} + \cos\theta_{max})/2$ with the cosine diference $\Delta\cos\theta \equiv \cos\theta_{min} - \cos\theta_{max}$ for 150 μL water drops pinned to a tilted surface with different initial contact angles (a): θ_0 = 60° (circles), 90° (squares), and 120° (diamonds). (b) Zoom of the case θ_0 = 60°. The symbols are Surface Evolver results, and the solid lines are quadratic fits to the data.

DOI: 10.1021/acs.langmuir.5b00834
Langmuir XXXX, XXX, XXX−XXX

b is a parameter that depends on θ_0, and V_r is a given reference volume. For simplicity, in our calculations, we took $V_r = 1\ \mu L$.

Figure 8 shows a plot of the results for $k_\infty(\theta_0)$ and $b(\theta_0)$ obtained in the linear fits of Figure 7. As one can see, k_∞ (circles) presents a cubic behavior with $\cos\theta_0$ while b (triangles) has a quadratic behavior with $\cos\theta_0$. Performing the corresponding fits to the data (see Figure 8), we obtain

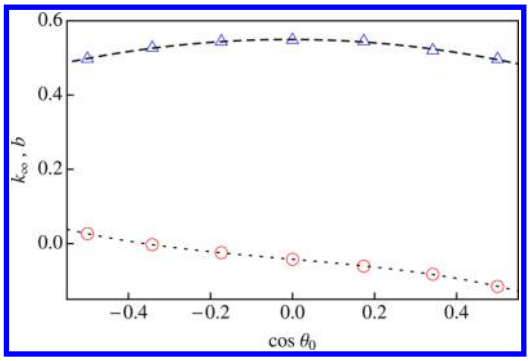

Figure 8. Parameters k_∞ (circles) and b (triangles) versus $\cos\theta_0$ for water drops pinned to a tilted surface. The symbols are obtained from the linear fits of Figure 7 (see text). The dashed line is a quadratic fit to the $b(\cos\theta_0)$ data, and the dotted line is a cubic fit to the $k_\infty(\cos\theta_0)$ data.

$$k_\infty(\theta_0) \cong -0.0421307 - 0.0964211\cos\theta_0 - 0.00845812\cos^2\theta_0 - 0.180876\cos^3\theta_0 \quad (20)$$

$$b(\theta_0) \cong 0.549691 - 0.00318195\cos\theta_0 - 0.21131\cos^2\theta_0 \quad (21)$$

where we would like to note that considering a different fluid instead of water would lead to different fits for k_∞ and b in terms of $\cos\theta_0$.

3.2. Direct Calculation of the Most Stable Contact Angle in a Tilted Drop. In the analysis presented in this section, we have considered a water drop with a circular triple line pinned to a tilted planar surface. In what follows, we shall see how the obtained results can be used to determine the most stable contact angle for a water drop with a given volume V in a surface with known advancing and receding contact angles θ_{adv} and θ_{rec}. The goal now is to determine the value of θ_0 compatible with $\theta_{min} = \theta_{rec}$ and $\theta_{max} = \theta_{adv}$. We shall denote this value as θ^C_{tilt}. In this case, eq 13 becomes

$$\langle\cos\theta\rangle_{a-r} \cong \cos\theta^C_{tilt} + k(\Delta\cos\theta)_{a-r}^2 \quad (22)$$

where

$$\langle\cos\theta\rangle_{a-r} \equiv \frac{\cos\theta_{adv} + \cos\theta_{rec}}{2} \quad (23)$$

$$(\Delta\cos\theta)_{a-r} \equiv (\cos\theta_{rec} - \cos\theta_{adv}) \quad (24)$$

and, using eq 18,

$$k = k(\theta^C_{tilt}, V) \cong k_\infty(\theta^C_{tilt}) + b(\theta^C_{tilt})\left(\frac{V}{V_r}\right)^{-0.6} \quad (25)$$

From eqs 22−25, using θ_{rec} and θ_{adv} as inputs, one can numerically obtain the most stable contact angle θ^C_{tilt}.

The above results imply that the most stable contact angle depends on the drop volume. This would be in contradiction with experiments[14] and the numerical results presented in Figure 4. However, for the relatively large volumes considered in Figure 4, $k \to k_\infty$ and we do not expect a relevant volume dependence. In particular, solving eqs 22−25 for the system of Figure 4, that is, water drops on uPVC ($\theta_{rec} = 50°$, $\theta_{adv} = 86°$) with volumes V = 100, 120, and 150 μL, we obtain θ^C_{tilt} = 67.99°,67.92°, and 67.84° respectively, with very small volume dependence and in close agreement with the results of Figure 4a.

Finally, we would like to note that assuming that $\cos\theta^C_{tilt}$ is close to $\langle\cos\theta\rangle_{a-r}$ one can derive the following first order approximation:

$$\cos\theta^{C,1}_{tilt} \cong \langle\cos\theta\rangle_{a-r} - \left[k_\infty(\langle\cos\theta\rangle_{a-r}) + b(\langle\cos\theta\rangle_{a-r})\left(\frac{V}{V_r}\right)^{-0.6}\right](\Delta\cos\theta)_{a-r}^2 \quad (26)$$

Equation 26 yields a very good approximation to the numerical solution of eqs 22−25 as one can observe in Table 1 where the values of θ^C_{tilt} and $\theta^{C,1}_{tilt}$ are very close for all of the considered polymer surfaces. Furthermore, we observe an excellent agreement with the values of θ^A_{tilt}.

4. SUMMARY

Inspired by the experimental tilting plate method for determining the most stable contact angle developed by Montes et al.,[14] in this work, we have performed a numerical analysis of this method by resorting to Surface Evolver calculations. The calculations have been performed using an algorithm recently developed by us[16] that allows for modeling contact angle hysteresis in the Surface Evolver framework. The algorithm is applicable to nonaxisymmetric drops and thus is suitable to deal with sessile drops in tilted surfaces.[17]

In a first approach to the problem, we have shown that the numerical calculations can reproduce the experimental results for the most stable contact angle in the tilting plate method with very good agreement in most cases. In this case, the most stable contact angle θ^A_{tilt} is obtained from the initial contact angle θ_0 related to the maximum value of the critical tilt angle α_1.

In a second approach to the problem, we have analyzed the evolution of the maximum and minimum contact angles in a sessile drop pinned to a tilted surface. This is the situation that arises for a drop with an initial contact angle equal to the most stable contact angle that is tilted until simultaneously reaching at the front and the rear of the drop the advancing and the receding contact angles, respectively. Although the cosines of the maximum and minimum contact angles are well approximated by linear fits in terms of $\Delta\cos\theta$, we have found that the cosine average $\langle\cos\theta\rangle$ has a well-defined quadratic behavior with $\Delta\cos\theta$, with a proportionality factor k that depends on the volume V and the initial contact angle θ_0 of the drop. Once the behavior of k in terms of V and θ_0 is obtained, the quadratic law for $\langle\cos\theta\rangle$ can be used to determine the most stable contact angle of a system with given advancing and receding contact angles by solving a nonlinear set of equations. The result of this approach, θ^C_{tilt}, is very close to θ^A_{tilt}, showing the consistency of both methods. Finally, a first order analytical approximation to θ^C_{tilt} has been

DOI: 10.1021/acs.langmuir.5b00834
Langmuir XXXX, XXX, XXX−XXX

derived with excellent agreement with the results of the other approaches.

AUTHOR INFORMATION

Corresponding Author

*E-mail: white@usal.es.

Present Address

[§]J.A.W.: Also at IUFFyM, University of Salamanca, Spain.

Notes

The authors declare no competing financial interest.

ACKNOWLEDGMENTS

We are thankful for financial support by Ministerio de Economía y Competitividad of Spain under Grant ENE2013-40644-R.

REFERENCES

(1) Young, T. An essay on the cohesion of fluids. *Philos. Trans. R. Soc. London* **1805**, *95*, 65−87.

(2) Marmur, A. Soft contact: Measurement and interpretation of contact angles. *Soft Matter* **2006**, *2*, 12−17.

(3) Lam, C. N. C.; Ko, R. H. Y.; Yu, L. M. Y.; Ng, A.; Li, D.; Hair, M. L.; Neumann, A. W. Dynamic cycling contact angle measurements: Study of advancing and receding contact angles. *J. Colloid Interface Sci.* **2001**, *243*, 208−218.

(4) Lam, C. N. C.; Kim, N.; Hui, D.; Kwok, D. Y.; Hair, M. L.; Neumann, A. W. The effect of liquid properties to contact angle hysteresis. *Colloids Surf., A* **2001**, *189*, 265−278.

(5) Lam, C. N. C.; Wu, R.; Li, D.; Hair, M. L.; Neumann, A. W. Study of the advancing and receding contact angles: Liquid sorption as a cause of contact angle hysteresis. *Adv. Colloid Interface Sci.* **2002**, *96*, 169−191.

(6) Eral, H.; 't Mannetje, D.; Oh, J. Contact angle hysteresis: A review of fundamentals and applications. *Colloid Polym. Sci.* **2013**, *291*, 247−260.

(7) Smith, T.; Lindberg, G. Effect of acoustic energy on contact angle measurements. *J. Colloid Interface Sci.* **1978**, *66*, 363−366.

(8) Andrieu, C.; Sykes, C.; Brochard, F. Average spreading parameter on heterogeneous surfaces. *Langmuir* **1994**, *10*, 2077−2080.

(9) Decker, E. L.; Garoff, S. Using vibrational noise to probe energy barriers producing contact angle hysteresis. *Langmuir* **1996**, *12*, 2100−2110.

(10) Meiron, T. S.; Marmur, A.; Saguy, I. S. Contact angle measurement on rough surfaces. *J. Colloid Interface Sci.* **2004**, *274*, 637−644.

(11) Mettu, S.; Chaudhury, M. K. Stochastic relaxation of the contact line of a water drop on a solid substrate subjected to white noise vibration: Roles of hysteresis. *Langmuir* **2010**, *26*, 8131−8140.

(12) Montes Ruiz-Cabello, F. J.; Rodríguez-Valverde, M. A.; Cabrerizo-Vílchez, M. A. Comparison of the relaxation of sessile drops driven by harmonic and stochastic mechanical excitations. *Langmuir* **2011**, *27*, 8748−8752.

(13) Montes Ruiz-Cabello, F. J.; Rodríguez-Valverde, M. A.; Cabrerizo-Vílchez, M. A. Equilibrium contact angle or the most-stable contact angle? *Adv. Colloid Interface Sci.* **2014**, *206*, 320−327.

(14) Montes Ruiz-Cabello, F. J.; Rodriguez-Valverde, M. A.; Cabrerizo-Vilchez, M. A new method for evaluating the most stable contact angle using tilting plate experiments. *Soft Matter* **2011**, *7*, 10457−10461.

(15) Brakke, K. The surface evolver. *Exp. Math.* **1992**, *1*, 141−165.

(16) Santos, M. J.; White, J. A. Theory and simulation of angular hysteresis on planar surfaces. *Langmuir* **2011**, *27*, 14868−14875.

(17) Santos, M. J.; Velasco, S.; White, J. A. Simulation analysis of contact angles and retention forces of liquid drops on inclined surfaces. *Langmuir* **2012**, *28*, 11819−11826.

(18) Chou, T.-H.; Hong, S.-J.; Sheng, Y.-J.; Tsao, H.-K. Drops sitting on a tilted plate: Receding and advancing pinning. *Langmuir* **2012**, *28*, 5158−5166.

(19) Janardan, N.; Panchagnula, M. V. Effect of the initial conditions on the onset of motion in sessile drops on tilted plates. *Colloids Surf., A* **2014**, *456*, 238−245.

(20) Semprebon, C.; Brinkmann, M. On the onset of motion of sliding drops. *Soft Matter* **2014**, *10*, 3325−3334.

(21) Korhonen, J. T.; Huhtamäki, T.; Ikkala, O.; Ras, R. H. A. Reliable measurement of the receding contact angle. *Langmuir* **2013**, *29*, 3858−3863.

(22) Krasovitski, B.; Marmur, A. Drops down the hill: Theoretical study of limiting contact angles and the hysteresis range on a tilted plate. *Langmuir* **2005**, *21*, 3881−3885.

DOI: 10.1021/acs.langmuir.5b00834
Langmuir XXXX, XXX, XXX−XXX